Chapter 2
Fundamentals

The basic principle of the STM experiment is described in Sect. 2.1. A theoretical basis for the treatment of electron tunneling in STM is given by Bardeen's theory [1], which is the preeminent quantitative theory of the tunneling current in STM [2]. It was published in 1961 and applied to the STM in 1983 by Tersoff and Hamann [3] (Sect. 2.2). The latter method is incorporated into nearly every state of the art density functional theory (DFT) code. A simpler model was proposed by Selloni et al. and Lang [4, 5], making use of the Wentzel–Kramers–Brillouin (WKB) approximation. This will be discussed with respect to Scanning Tunneling Spectroscopy (STS) (Sect. 2.3). A discussion about the contrast mechanism of organic adsorbates on solid surfaces in STM images is presented in Sect. 2.4. Other experimental methods, which were used in the work at hand are Temperature Programmed Desorption (TPD) (Sect. 2.5) and Low Energy Electron Diffraction (LEED) (Sect. 2.6).

2.1 Principle of the STM

With the invention of the STM in 1982 by Binnig and Rohrer et al. [6] it became possible to investigate not only the topography of a conducting sample with atomic resolution in real space, but also the local electronic properties. The principle of the STM is based on the quantum-mechanical effect of electron tunneling. This allows an electron to tunnel through a potential barrier even though its classical kinetic energy is lower than the barrier height. This specific process can occur between two materials which are separated by a gap, forming a potential barrier for the electrons. Commonly conductors and/or semiconductors are used as substrates; however, it is noteworthy to mention that ultrathin layers of an isolating material can also be imaged by STM [7, 8].

F. Buchner, *STM Investigation of Molecular Architectures of Porphyrinoids on a Ag(111) Surface*, Springer Theses, DOI: 10.1007/978-3-642-14840-8_2,

A metallic tip (e.g., platinum iridium (90:10), or tungsten) is used as the probe and approached towards the surface until a tunnelling current flows, when a voltage is applied between the tip and the sample. This occurs when the gap between the tip and the surface is in the order of roughly 1 nm. After the tunnelling contact is established, the tip scans over the surface, actuated by a piezoelectric scanning unit, whose extension can be controlled in three dimensions x, y and z. This can be realized by applying a specific voltage to the piezoelectric elements of the scanner. Such a microscope is typically capable of recording micrographs of an area of a few nm up to several μm.

The distance-dependent nature of the tunneling current is essential for the discrimination of very small surface corrugations (i.e., atomic corrugation of a single crystalline metal surface), since even small changes generate a large change in the tunneling current. The quantum mechanical treatment predicts an exponential decay for the wave function of the electron in the barrier. For a rectangular barrier, the probability of the tunneling process decreases exponentially with the distance d between the tip and the sample and with increasing barrier height. The tunneling current I_T can be estimated by Eq. 2.1 (at low voltage and temperature; the tunneling direction is specified by the polarity of the applied bias voltage) [9]:

$$I_T \propto U \exp(-2d\kappa); \kappa = \sqrt{\frac{2m_e\phi}{\hbar^2}}. \tag{2.1}$$

ϕ is the average barrier height $1/2(\phi_{\text{sample}} + \phi_{\text{tip}})$ between the two electrodes, m_e is the electron mass and κ is the inverse decay length. Due to the exponential dependency of the tunneling current a vertical resolution of up to 0.01 Å can be achieved. The lateral resolution is lower by a factor of roughly 10; it is determined by the radius of the tip, which ideally exhibits the dimension of only one tip atom.

A three-dimensional STM data set of a surface can be recorded with two different operation modes [9]. Firstly, in both modes, the scanning tip is navigated close to the surface, so that at a certain bias voltages (typically $U_{\text{Bias}} \sim 5$ mV to 2 V) a tunneling current (typically 5 pA to 2 nA) is detectable. In the constant current mode, the tip is scanned over the surface, while the tunneling current I_T, between the tip and the surface, is sensed. A feedback loop controls the height of the tip $z(x, y)$ (realized with the z-piezo actuator), in such a way that the current remains constant. Thus, an image consists of a map $z(x, y)$ of tip height versus lateral position x, y.

Alternatively, in the constant height mode the tip is scanned across the surface at constant height and constant bias voltage. In this case, the tunneling current $I(x,y)$, measured at discrete scan positions x,y constitutes the data set. This mode is advantageous as it allows high scan speeds (low record time per image) and thus avoids large thermal drifts. However, it is limited to very flat surfaces or/and very small scanning areas, as massive surface defects or extended contaminations can cause a crash of the tip.

2.2 Origin of the Tunneling Current

Since electron tunneling occurs from or into electronic states near the Fermi level, which can exhibit a complex structure, it is obvious that the electronic structures of the surface and the tip play a major role determining the tunneling current. Note that the energy range of this process is given by the applied bias voltage.

In early analyses, the one-dimensional tunneling problem has been treated extensively [10]; however, few considerations were made in three dimensions. Yet these were desirable in order to interpret STM micrographs. With this respect, in 1983 a theory was developed by Tersoff and Hamann, which is still the standard today. It is based on Bardeen's Transfer Hamiltonian Theory and was introduced to explain Giaver's observations of tunneling in systems of superconducting electrodes separated by thin oxide barriers [1]. This specific approach had the advantage of describing the many-particle nature of the tunnel junction. In the model, a weak overlap of the wave functions of the surface states of the two electrodes allowed a first-order perturbation calculation. By summation over all states within a given energy interval eV from the Fermi level, the tunneling current I_T in Bardeen's formalism is given by [1]:

$$I_T = \frac{2\pi|e|}{\hbar}\sum_{\mu,v}[1 - f(E_v + eV)] \times /M_{\mu v}/^2 \delta(E_v - E_\mu) \tag{2.2}$$

$M_{\upsilon v}$ is the tunneling matrix element between the eigenstates ψ_μ and χ_v, $f(E)$ is the Fermi function, V is the voltage across the barrier, E_μ is the energy of the state μ, E_v is the energy of the state v.

The indices run over all the states of the surface μ and the tip v. Exclusively elastic tunneling transition is allowed by means of the δ-function, i.e., electrons can only tunnel, if there is an unoccupied state with the same energy in the other electrode. When assuming low bias voltages ($\sim$10 meV for metal–metal tunneling, which is much smaller than the average work function, the expression simplifies to [11]

$$I_T = \frac{2\pi}{\hbar}e^2 V \sum_{\mu,v} /M_{\mu v}/^2 \delta(E_\mu - E_F)\delta(E_v - E_F). \tag{2.3}$$

Bardeen [1] showed, that the tunneling matrix element $M_{\mu\upsilon}$ can be written in a form, which only requires knowledge of the wave functions of the two electrodes separately. The matrix element $M_{\mu\upsilon}$ in Eq. 2.3 can be expressed as

$$M_{\mu v} = \langle \psi_\mu | H_T | \chi_v \rangle = -\frac{\hbar^2}{2m_e}\int (\psi_\mu^* \nabla \chi_v - \chi_v \nabla \psi_\mu^*)\, dS \tag{2.4}$$

$M_{\upsilon v}$ is the tunneling matrix element between the eigenstates ψ_μ and χ_v of the two electrodes, containing the transition probability between the two systems. The integral covers any surface lying in the barrier region between the tip and the sample.

Tersoff and Hamann applied Bardeen's formula to the STM, assuming that the tip wave function is of s-type. Thus the following expression for the tunneling current I_T in the limit of zero temperature and very low bias was found [11]:

$$I_T = 32\pi^3\hbar^{-1}e^2V\Phi^2\rho_t(E_F)R^2\kappa^{-4}e^{2\kappa R} \times \sum_v /\psi_v(\vec{r_0})/^2\delta(E_v - E_F)$$
$$\rho_s(r_0, E_F) \equiv \sum_\mu /\psi_v(\vec{r_0})/^2\delta(E_v - E_F). \tag{2.5}$$

R is the tip radius, ρ_t is the density of states per volume of the probe tip, ρ_s is the density of states per volume of the sample

In this equation, the tunneling current depends e.g., on the average work function Φ and on the density of states ρ_t of the tip at the Fermi level. The sample properties are given by the value of the sample wave function ψ_v with an energy E_v at the center of curvature r_0 of the tip, constituting the LDOS [12]. Thus the LDOS represents the charge density per unit energy at E_F at a certain point above the surface [11]. Tersoff and Hamann showed that Eq. 2.5 remains valid, regardless of tip size, as long as the tunneling matrix elements can be adequately approximated by an s-orbital tip wave function.

It is noteworthy to mention that in this approach it was not intended to accurately describe a real tip, but to find a way to parametrize the effect of a finite tip size [13]. However, experimentally in particular tungsten or platinum iridium tips were used as probes to achieve high-resolution STM images of well defined metal surfaces. In terms of actual tip states, these tip materials exhibit a localized d_{z^2} character near the Fermi energy and were proposed by Chen [13] to be favorable to achieve atomic resolution. Furthermore, with respect to imaging semiconductor surfaces i.e., Si(111)7 × 7, it was assumed that the tip may pick up a silicon cluster to form a p_z dangling bond state at the tip which might then play a role in achieving atomically resolved STM images. Later on, extensions of the Tersoff-Hamann model were developed, making use of the Modified Bardeen Approach (MBA), e.g., different tip states were included.

Obviously, it is challenging to interpret STM images, taking into account the factors that contribute to the tunneling current. The apparent height $z(x,y)$ in the micrographs can either be understood in terms of topography and/or electronic effects of the substrate and the adsorbate on the latter. Several examples, which highlight this discrepancy have been reported in literature, e.g., the STM images of highly oriented pyrrolytic graphite (HOPG), where every second carbon atom of the uppermost layer, which has no direct neighbour in the layer below, exhibits an increased apparent height [14]. The observation is attributed to a lower LDOS of those atoms that interact with carbon neighbours directly underneath. Oxygen atoms on Pd(111) appear concave in the micrographs, even though they are topographically convex. This was traced back to the high electronegativity of oxygen. It was shown by Tilinin et al. [15] that as the electronegativity decreases (from the element fluorine to carbon), the depressions gradually switch into a shallow dimple in the case of nitrogen and into a protrusion for carbon. Thus, it is

noteworthy to mention that theoretical modelling of STM images (e.g., Hückel theory, density field theory, electron scattering quantum chemistry) in combination with the experiment can be helpful.

2.3 Scanning Tunneling Spectroscopy

As demonstrated in Sect. 2.2, an STM image presents a convolution of both topography and electronic structure of a surface. With the STM operating in the spectroscopy mode, the electronic information can be separately recorded by scanning tunneling spectroscopy (STS) [9]. By doing so, scanning is interrupted and the tip is positioned over a region of interest in a distance adjusted by the feedback circuit accordingly to the applied tunneling resistance. It is conducted by opening the feedback loop, followed by ramping the bias voltage V to measure the tunneling current I as a function of applied bias $I(V)$. The extraction of the electronic information is carried out by calculating the derivative $\partial I/\partial V$, i.e., the differential conductivity, which is proportional to the local density of states (LDOS) [12].

For a discussion of the recorded $I(V)$ curves, it has to be taken into account that the theory of Tersoff and Hamann is restricted to very low bias voltages, as typically applied for imaging inorganic samples. However, many organics on solid supports exhibit a gap between the highest occupied molecular orbital (HOMO) and the lowest unoccupied molecular orbital (LUMO) (i.e., HOMO-LUMO gap) in the order of 1 eV, which means that the assumption $V \approx 0$ is inappropriate. For that purpose and thereupon for applying a simpler model, the theory of three-dimensional tunneling based on the transfer-Hamiltonian formalism has been reconsidered by Selloni et al. [4] and Lang et al. [5].

The theory proposed by Lang et al. [5] makes use of the model of a one-dimensional tunnel junction in the Wenzels–Kramer–Brillouin (WKB) approximation, which was found to be in good agreement with the transfer Hamiltonian calculation, regarding qualitative features [5, 12]. It was recently demonstrated by Wagner et al. [12] and Koslowski et al. [16] that using the WKB approach, the DOS can be recovered in an energy range of roughly ± 2eV. The tunneling current can be expressed by the integral over the density of states (DOS) of both sample ρ_t and tip ρ_S and the transmission function T.

$$I(d,V) \cong \frac{2\pi e}{\hbar}\left(\frac{\hbar^2}{2m}\right)\int_0^{eV} T(d,V;E)[f(E-eV)-f(E)]\rho_S(E)\rho_t(E-eV)\mathrm{d}E. \quad (2.6)$$

Note that the one dimensional WKB approach does not consider the wave functions of the electrodes, just as in the Tersoff–Hamann model. Here the density of electronic states is taken into account and combined in a transmission function $T(d,V;E)$, depending on the energy of the electrons, the applied voltage and the distance. For a trapezoidal barrier in one dimension the transmission probability can be approximated by:

$$T(d,\Phi_{S,T},V;E)\cong\exp\left[-2(d+R)\frac{2}{3}\sqrt{\frac{2m}{\hbar^2}\times\left(\frac{(\Phi_t-E+eV)^{3/2}-(\Phi_S-E)^{3/2}}{\Phi_t-\Phi_s+eV}\right)}\right] \tag{2.7}$$

R is the radius of a local spherical tip, with the center of the curvature at a distance d.

Tersoff and Hamann [3] demonstrated that the LDOS represents the charge density per unit energy at E_F at a centain point above the surface. Equation 2.5 also implies that the differential conductivity $\partial I/\partial V$ is proportional to the sample $LDOS(E_F)$ near the Fermi energy (i.e., for very small bias voltages). For higher bias voltages, with respect to the one-dimensional WKB approach, the energy- and bias-dependent electron transition probability is implied in the transmission function $T(r_0,V,E)$ and thus can also be seen as a measure of the charge density of each state that reaches r_0. Thus the quantity

$$\frac{\partial I}{\partial V}\propto T(r_0,V;E)\rho_S(E)\overset{1D-WKB}{\equiv}LDOS. \tag{2.8}$$

is a generalized LDOS at r_0 in terms of the Tersoff–Hamann model [12]. Note that the WKB approach is an approximation due to the voltage-dependence of the transmission. By applying small bias voltages, a constant transmission function and a constant sample density of states can be assumed. Thus it can be concluded:

$$\frac{\partial I}{\partial V}\propto DOS\propto LDOS. \tag{2.9}$$

In particular with respect to inorganic surfaces, Stroscio et al. [17] considered a normalization of the differential conductivity in order to divide out large part of the transmission probability T.

$$\frac{\partial I}{\partial V}\Big/\frac{I}{V}=\frac{\mathrm{d}\ln I}{\mathrm{d}\ln V} \tag{2.10}$$

However, nowadays this method is not routinely applied to organic adsorbate layers, as it was originally used to determine the DOS for inorganic surfaces. Furthermore, it potentially induces singularities in the energy gap around E_F and undesired peak shifts. Thus it can be seen more or less as a mathematical method for peak detection, which has to be applied carefully. Alternative methods for DOS recovery were supposed e.g., by Ukraintsev [18], Wagner et al. [12] and Koslowski et al. [16].

2.4 Contrast Mechanism of Molecular Adsorbates

In the past, STM measurements have mostly been performed to acquire micrographs of flat metal and semiconductor surfaces with atomic resolution. Meanwhile, STM has become a well-established tool for imaging a variety of organic

molecular adsorbates. The contrast mechanism of the latter was both interpreted in terms of an adsorbate induced change of the local work function [19] and by molecule-mediated electron transport through orbital channels [20, 21].

It has been shown by Spong et al. [19] that different functional groups attached to the same aromatic core can be distinguished with STM. The observation has been related to the modulation of the local work function of the substrate, induced by adsorbate molecules or fragments. In particular for 5-nonyl-2-*n*-nonoxyl-phenylpyrimidine, 4-cyano-4-*n*-butoxyl-biphenyl and 4-(4-*n*-propyl-cyclohexyl)-cyano-cyclohexane, it was proposed that the contrast cannot be interpreted by resonant tunneling, since the molecular levels are too far from the Fermi level (assuming weak adsorption) to be accessible by STM.

The magnitude of the tunneling current is sensitive both to changes in the local work function and the distance; consequently changes of material and topography can be detected. A polarizable molecule or part of it, exposed to the electric field inside the tunneling barrier modifies the work function and in turn changes the barrier height Φ. Thereby the local barrier height of a clean surface, ϕ is altered,

$$\Phi = \phi - e\mu/\varepsilon_O \tag{2.11}$$

with μ being the dipole moment density of the adsorbed species, e the electronic charge and ε_0 the permittivity of free space. The dipole moment of the adsorbed species can both be permanent, μ_P or induced (μ_I) by an electric field E through its polarizability α:

$$\mu = \mu_P - \mu_I(\alpha, E) \tag{2.12}$$

It was shown, that the alkyl tails of the above mentioned molecules adsorbed on highly oriented pyrolytic graphite appear dimmer in constant current images than the aromatic center. The observation was proposed to be due to lower polarizability and consequently less modification of the local work function of the aromatic entity [19]. Thus, regarding adsorbate molecules for which the frontier molecular energy levels are located well above or below the Fermi level, the observed constant current images can be interpreted in terms of the local variation of the work function Φ, modified by the permanent and/or the induced dipole moment of physisorbed molecules.

The individual molecular appearance can also be interpreted in terms of the distribution of the electron density in the frontier molecular orbitals of the adsorbate. An additional tunneling contribution, e.g., observable as peak in STS data, contributes when the energy of the tunneling electron equals the energy of a molecular orbital of the adsorbed molecule. Thereby an electron channel through the respective orbital is opened up, resulting in an increase of the tunneling current. The process is referred to as resonant or orbital mediated tunneling (OMT) [12, 20, 21].

Taking into account an adsorbate molecule, the tunneling barrier can be described as one-dimensional and rectangular including an inserted potential well (Fig. 2.1a) [21]. It is proposed that the molecule exhibits discrete energy levels

inside the well (indicated by the HOMO and the LUMO). The first barrier exists between STM tip and molecule w_1, the second one between adsorbate and substrate w_3. The Fermi energy of the sample E_{FS} and the tip E_{FT} exhibit no potential difference in the case of tunneling contact and zero bias voltage condition.

The energy schemes (Fig. 2.1b, c) highlight the principle of orbital mediated tunneling with respect to positive bias voltages applied to the sample. This means that electrons tunnel from occupied states of the tip into unoccupied states of the sample. If an energy $eU = E_{LUMO}$ is applied to the tunneling junction, a potential difference between the Fermi energies of the two electrodes is induced (Fig. 2.1b).

V indicates the LUMO′s energy level measured from the Fermi energy under zero-bias conditions. It is obvious that the applied energy eU is smaller than the amount $V + \Delta$, i.e., no resonant amplification of the tunneling current occurs. The electric field gradient through the tunneling junction is taken into account by the amount Δ, depending on the position of the molecule inside the barrier, e.g., $w_3 = 0; \Rightarrow \Delta = 0$, assuming a symmetric position inside the barrier $w_3 = w_1; \Rightarrow \Delta = a$. In this respect, Δ represents bias voltage induced shift of the orbital of interest. The amount of the shift and therefore the peak position in STS can be expressed by

$$V_{Peak} = V + \frac{1/2w_2 + w_3}{w_1 + 1/2w_2} V \tag{2.13}$$

The energy of at least $V + \Delta$ has to be applied (Fig. 2.1c) to observe a significant increase in the tunneling current. Thereby, the transmission probability increases, induced by mediated tunneling through the LUMO (indicated by the arrow).

By applying a negative bias voltage electron tunneling occurs from occupied states of the sample into unoccupied states of the tip. At an appropriate bias voltage OMT takes place through the HOMO (indicated by the grey arrow in Fig. 2.1d) and is observable as an increase of the tunneling current as well.

2.5 Temperature Programmed Desorption

TPD spectroscopy was a prerequisite for the preparation of well defined monolayers, as it was essential to determine the temperature, which is adequate to desorb multilayer porphyrinoids, but too low to desorb the monolayer molecules. Thus basic considerations of TPD will be given in this chapter. In the experiment a certain molecular coverage is generated on the sample, followed by subsequent annealing with a constant temperature ramp to desorb the molecules. The detection of desorbing particles is achieved by a quadrupole mass spectrometer, which allows the plotting of the intensity against the temperature. Thermal desorption is often described by an Arrhenius expression, which is also referred to as Polanyi–Wigner equation [22].

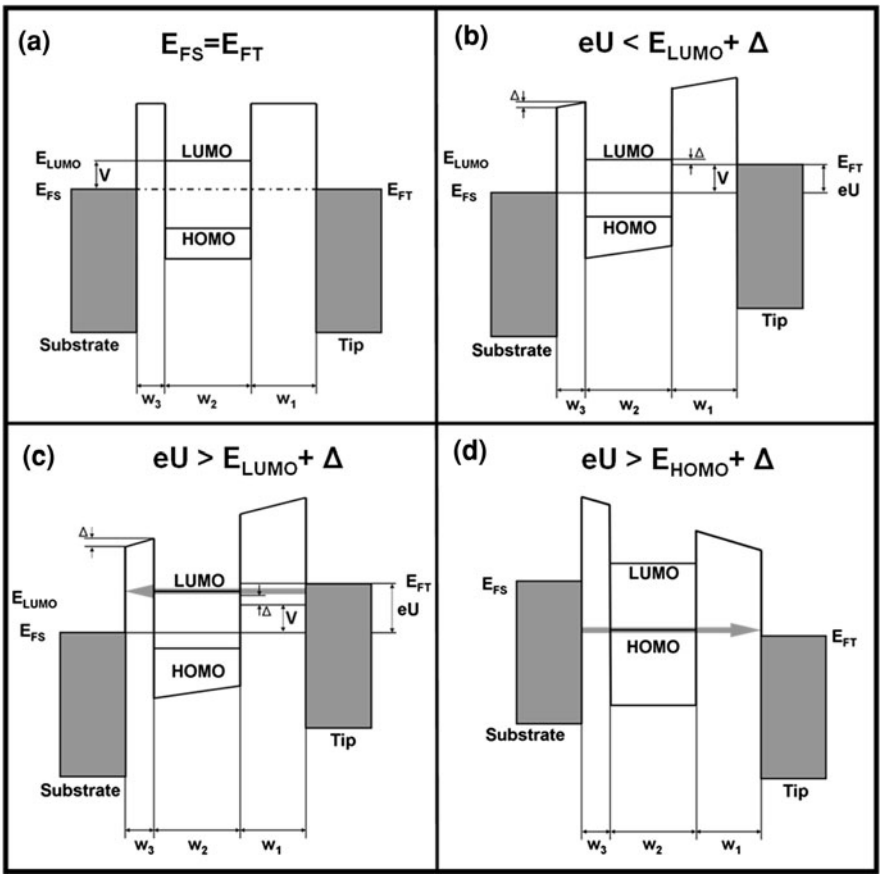

Fig. 2.1 **a** Tunneling junction at zero bias conditions. The adsorbed molecule is represented by an inserted potential well inside the barrier. **b** An energy of $eU < V + \Delta$ is applied to the tunneling junction. **c** At an energy, $eU > V + \Delta$, mediated tunneling through the LUMO is observable (indicated by the *arrow*). **d** Mediated tunneling through the HOMO is observable by applying appropriate negative bias voltages (depicted by the *arrow*)

$$r_{\text{des}} = \frac{\partial\theta}{\partial T} = v(\theta) \cdot \theta^n \cdot \exp\left(-\frac{E_D(\theta)}{k_B T}\right) \tag{2.14}$$

θ is the coverage, T is the temperature, v is the preexponential factor, E_D is the desorption energy, k_B is the Boltzmann constant, n is the order of desorption, r_{des} is the desorption rate

Both the position and the shape of the peaks in TPD spectra can be analyzed, with the shape determining the order of desorption. 0th order is typically observable for multilayer desorption. In this case, the desorption rate r_{des} is independent of the coverage θ. 1st order desorption is found in the case of a monolayer, where the participating particles exhibit no lateral interactions. The desorption rate is

directly proportional to the coverage. 2nd order desorption can be observed in the case of reactions in the monolayer, followed by subsequent desorption.

Numerous ways to analyze TPD spectra have been proposed in literature. One route to evaluate the activation energy of desorption is given by the Redhead equation [23], utilizing solely the temperature of the desorption maximum T_m. This assumes that v and E_D are independent of the coverage θ. The derivative of the Polanyi–Wigner equation against the temperature T (assuming $n = 1$) results in

$$E = RT_m \left[\ln\left(\frac{vT_m}{\beta}\right) - 3.46 \right] \tag{2.15}$$

To evaluate desorption energies typically preexponential factors v of 10^{13} are taken into account.

Another way to determine desorption energies is the Habenschaden–Küppers or leading-edge analysis [24], assuming that the preexponential factor v is independent of the coverage. In that course, a small interval of the TPD spectrum in the region of the low temperature and high coverage side is taken into the analysis, to ensure insignificantly (<5%) variations of θ. Thus, this method is appropriate to calculate desorption energies in the case when the coverage does not change significantly. For this purpose, the logarithm of the Polanyi–Wigner equation is applied:

$$\ln r_{des} = \ln v + \ln \theta^n - \frac{E_{des}}{RT} \tag{2.16}$$

By plotting a spectrum as $\ln r_{des}/\theta^n$ against $1/T$, a straight line can be obtained with the slope of $m = E_{des}(\theta)/R$, from which the desorption energy can be calculated. For 0th order this equation holds over the complete desorption spectrum.

2.6 Low Energy Electron Diffraction

Low energy electron diffraction (LEED) is a well-established tool to determine the geometric structure of both single crystalline surfaces and adsorbed phases under UHV conditions. In LEED, electrons are accelerated to kinetic energies in the range of 20 to 500 eV and hit the sample perpendicular. In contrast to X-rays, which can be used for bulk structure analysis, these electron exhibit a low mean free path in a solid, thus giving information of the uppermost layers. The electrons wavelength is given by de Broglies equation:

$$\begin{aligned} \lambda = \frac{\hbar}{mv}; E_{Kin} = \frac{1}{2}mv^2 = eU; \\ \Rightarrow \lambda = \frac{\hbar}{\sqrt{2m_e eU}} \end{aligned} \tag{2.17}$$

The corresponding de Broglie wave length of 0.3–0.05 nm is in the range of inter-atomistic and/or inter-molecular dimensions. Therefore, surface atom or adsorbate induced diffraction of electrons occurs. In the LEED experiments, the diffraction spots are observed on a fluorescence screen; they represent a projection of the reciprocal space. This allows the drawing of conclusions on the size and shape of the real space unit cell of a surface or molecular layer.

References

1. Bardeen J (1961) Phys Rev Lett 6:57
2. Gottlieb AD, Wesoloski L (2006) Nanotechnology 17:R57
3. Tersoff J, Hamann DR (1983) Phys Rev Lett 50:1998
4. Selloni A, Carnevali P, Tosatti E, Chen CD (1985) Phys Rev B 31:2602
5. Lang ND (1986) Phys Rev B 34:5947
6. Binnig G, Rohrer H, Gerber C, Weibel E (1982) Phys Rev Lett 49:57
7. Simic-Milosevic V, Heyde M, Nilius N, König T, Rust H-P, Sterrer M, Risse T, Freund H-J, Giordano L, Pacchioni G (2008) J Am Chem Soc 130:7814
8. Ramoino L, von Arx M, Schintke S, Baratoff A, Güntherodt H-J, Jung TA (2006) Chem Phys Lett 417:22
9. Hansma PK, Tersoff J (1987) J Appl Phys 61:R1
10. Duke CB (1969) Tunneling in solids. Academic Press, New York
11. Tersoff J, Hamann DR (1985) Phys Rev B 31:805
12. Wagner C, Franke R, Fritz T (2007) Phys Rev B 75:235432
13. Chen CJ (1990) Phys Rev Lett 65:448
14. Tománek D, Louie SG (1988) Phys Rev B 37:8327
15. Tilinin IS, Rose MK, Dunphy JC, Salmeron M, Van Hove MA (1998) Surf Sci 418:511
16. Koslowski B, Dietrich C, Tschetschetkin A, Ziemann P (2007) Phys Rev B 75:035421
17. Stroscio JA, Feenstra RM, Fein AP (1986) Phys Rev Lett 57:2579
18. Ukraintsev VA (1996) Phys Rev B 53:11176
19. Spong JK, Mizes HA, LaComb LJ Jr, Dovek MM, Frommer JE, Foster JS (1989) Nature 338:137
20. Nazin GV, Wu SW, Ho W (2005) Proc Natl Acad Sci USA 102:8832
21. Mizutani W, Shigeno M, Kajimura K, Ono M (1992) Ultramicroscopy 42–44:236
22. de Jong AM, Niemantsverdriet JW (1990) Surf Sci 233:355
23. Redhead PA (1962) Vacuum 12:203
24. Habenschaden E, Küppers J (1984) Surf Sci 138:L147

http://www.springer.com/978-3-642-14839-2

STM Investigation of Molecular Architectures of Porphyrinoids on a Ag(111) Surface
Supramolecular Ordering, Electronic Properties and Reactivity

Buchner, F.

2010, XXVII, 164 p., Hardcover
ISBN: 978-3-642-14839-2